

Redox Control of Charge Transport in Vertical Ferrocene Molecular Tunnel Junctions

Chuancheng Jia^{1†}, Iain Grace^{2†}, Peiqi Wang^{1,3}, Abelkareem Almeshal², Zhihong Huang³, Yiliu Wang¹, Peng Chen¹, Laiyuan Wang¹, Jinyuan Zhou¹, Ziyang Feng¹, Zipeng Zhao³, Yu Huang^{3,4}, Colin J. Lambert^{2*} and Xiangfeng Duan^{1,4*}

¹Department of Chemistry and Biochemistry, University of California, Los Angeles, Los Angeles, CA 90095, USA.

²Physics Department, Lancaster University, Lancaster LA1 4YB, UK.

³Department of Materials Science and Engineering, University of California, Los Angeles, Los Angeles, CA 90095, USA.

⁴California NanoSystems Institute, University of California, Los Angeles, Los Angeles, CA 90095, USA.

[†]These authors contributed equally to this work

*To whom correspondence should be addressed. e-mail: xduan@chem.ucla.edu; c.lambert@lancaster.ac.uk

Controlling charge transport through molecular tunnel junctions is of crucial importance for exploring basic physical and chemical mechanisms at the molecular level and realizing the applications of molecular devices. Here, through a combined experimental and theoretical investigation, we demonstrate redox control of cross-plane charge transport in a vertical gold/self-assembled monolayer (SAM)/graphene tunnel junction composed of a ferrocene-based SAM. When an oxidant/reductant or electrochemical control are applied to the outside surface of the neutral single-layer graphene top electrode, reversible redox reactions of ferrocene groups take place with charges crossing the graphene layer. This leads to counter anions on the outer surface of graphene, which balance the charges of ferrocene cations in the oxidized state. Correspondingly, the junctions switch between a high-conductance, neutral state with asymmetrical characteristics and low-conductance, oxidized state with symmetrical characteristics, yielding a large ON/OFF ratio (>100). This robust control of charge transport in vertical molecular junctions by utilizing the electronic transparency of graphene provides a new route for realizing new functionalities in future molecular electronic devices.

Subject terms: Molecular junctions • Graphene • Confined redox reaction • Charge transport

Charge transport through single or self-assembled monolayer (SAM) of molecules has attracted great interest in the past two decades¹⁻⁴, due to the potential applications of molecular tunnel junctions, beyond current scaling limits, as diodes^{5,6}, switches^{7,8} and transistors^{9,10}. Furthermore, charge tunneling transport underpins basic physical and chemical mechanisms at the molecular level, such as room-temperature quantum interference (QI) effects¹¹⁻¹⁴, thermoelectricity¹⁵ and dynamic chemical processes^{16,17}. Recently, we have demonstrated a new design of vertical molecular tunneling junctions based on Au/SAM/graphene heterostructures^{13,14}, where single-layer graphene (SLG) acts as the top electrode and electricity flows in a cross-plane direction, perpendicular to the SAM. Since the SLG exhibits both partial electrical transparency^{18,19} and selective material permeability²⁰, we were motivated to determine if charge transport and chemical and electrochemical reactions could be separated across the graphene layer. Here, we demonstrate this unique capability by constructing a vertical tunnel junction composed of a ferrocene (Fc) based SAM, whose functionality relies on the separation of chemical or electrochemical redox reactions across the SLG.

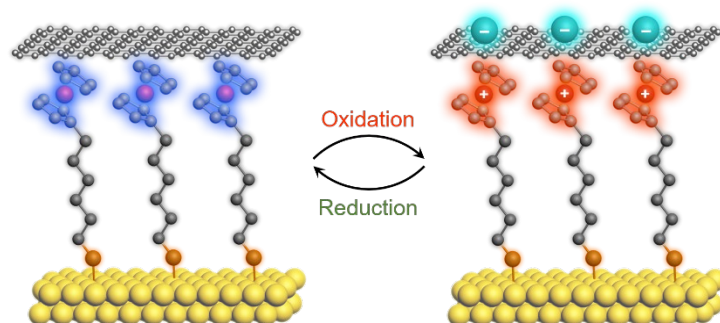


Fig. 1 | Redox dominant Au/Fc-SAM/SLG junction. Schematic illustration of the Au/Fc-SAM/SLG junction with oxidation and reduction treatments.

When an oxidant/reductant or electrochemical control are applied to the top of graphene, redox reactions of Fc groups beneath the graphene take place. After an oxidation process, counter anions exist on the outer surface of graphene to balance the charges of Fc cations in the oxidized state (Fig. 1), leading to a switch-off of charge transport through the junction switches with large ON/OFF ratio (>100). The designed vertical molecular tunnel junction can be utilized to explore novel chemical and electrochemical reactions at heterointerfaces, which are sensitive to the electronic

transparency of graphene, thereby imparting new functionalities to molecular-scale electronic devices.

The vertical molecular tunnel junction (Fig. 2a) is constructed as described in our previous works^{13,14}. Specifically, an ultra-flat Au film is deposited on the surface of highly doped silicon in a small hole at the center of a silicon/SiO₂ chip, where the conducting silicon can be used as source electrode for the final device. To incorporate the Fc-SAM, a monolayer of 6-ferrocenylhexanethiol (FcC₆S) is then self-assembled on the surface of Au film and confirmed by X-ray photoelectron spectroscopy (XPS) and electrochemical characterization²¹ (Supplementary Figs. 1 and 3). Chemical vapor deposition (CVD)-grown, single-layer graphene, confirmed by Raman characterization²² (Supplementary Fig. 4a), is then transferred and patterned on the top of Fc-SAM. Finally, a Ti/Au electrode is thermally deposited on the chip with one end around the graphene sheet, and a small amount of reactive solution or electrolyte solution is dropped on the top of Au/Fc-SAM/SLG channel. Since encapsulation by the graphene layer prevents direct contact between the Fc-SAM and the solution, the chemical redox reactions between the oxidant/reductant and Fc groups across graphene layer can be investigated. Furthermore, by adding patterned reference and counter Pt electrodes to the electrolyte solution, electrochemical redox reactions of Fc groups under graphene layer can be controlled.

The experimental current density (J_D) vs. bias voltage (V_D) for the junction in the initial state (before adding the oxidant) is shown in Fig. 2c (black line). An obvious asymmetry of the J_D - V_D curve with a rectification ratio ($R = |J(-0.8 \text{ V})|/|J(+0.8 \text{ V})|$) of ~ 14 can be observed. To achieve chemical oxidation (C-oxidation), a drop of 0.1 M H₂O₂ solution is added on top of Au/Fc-SAM/SLG, maintained for 2 h and blown away before further electrical measurements. From the experimental J_D - V_D curve of the C-oxidation treated state, it can be observed that the curve changes to a symmetric shape and the value of J_D decreases markedly (Fig. 2c, red line). In particular, at a negative bias ($V_D < 0 \text{ V}$), the J_D drops by over two orders of magnitude. Next, a drop of 0.1 M NaBH₄ solution is added on top of the chip, maintained for 2 h and blown away for

chemical reduction (C-reduction). After such a C-reduction treatment, the J_D-V_D characteristics of the device almost recovers to its initial state (Fig. 2c, green dotted line). When the device is sequentially treated by oxidizing and reducing solutions, it reversibly switches between a low conductance state after C-oxidation and high conductance after C-reduction (Supplementary Fig. 6). As a measure of this switching, in response to alternating chemical oxidation and reduction treatments, the $|J_D|$ at $V_D = -0.5$ V changes between low and high states with ON/OFF ratio of ~ 120 (Fig. 2d).

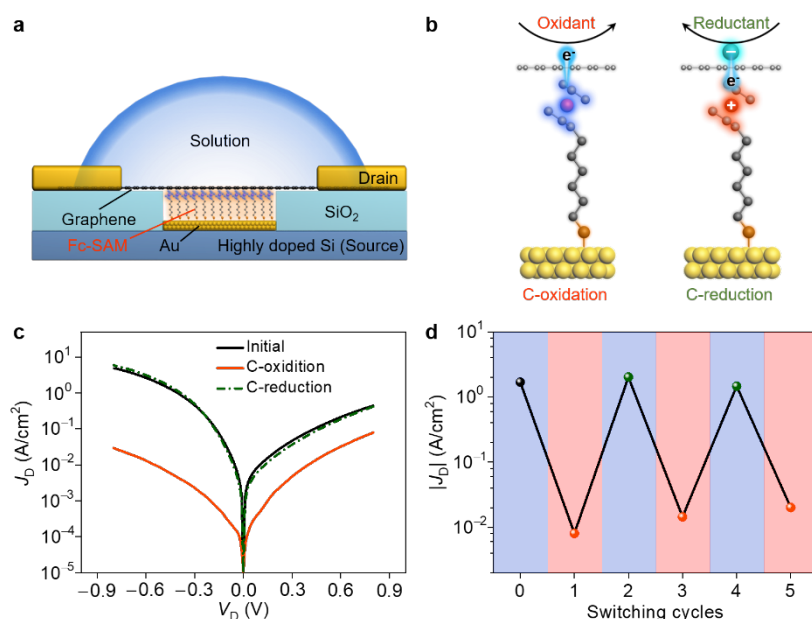


Fig. 2 | Chemical redox reactions of the junction. **a**, Schematic illustration of the device structure of Au/Fc-SAM/SLG junction with a liquid drop on top of the chip. **b**, Schematic illustration of chemical oxidation (C-oxidation) and chemical reduction (C-reduction) of Fc group in the junction with crossing graphene layer. **c**, Plots of experimental current density (J_D) vs. bias voltage (V_D) for the device in initial state, treated by H₂O₂ oxidizing solution (C-oxidation) and re-treated by NaBH₄ reducing solution (C-reduction). **d**, Corresponding $|J_D|$ at $V_D = -0.5$ V for the device sequentially treated by oxidizing (red) and reducing (green) solutions.

To explore the mechanism of such chemical treatments, similar Au/Fc-SAM/SLG samples with large areas were treated by the same oxidizing and reducing solutions. From XPS characterizations, it can be observed that most Fc groups are oxidized after H₂O₂ oxidizing solution treatment, especially as the large Fe³⁺ peaks appear in the Fe (2p) region (Supplementary Fig. 2a). When the sample is re-treated by a NaBH₄ reducing solution, the oxidized Fc⁺ groups are reduced to their initial state, as the Fe³⁺

peaks disappear (Supplementary Fig. 2b). From contact angle characterizations, it can be observed that the surface of Au/Fc-SAM/SLG becomes more hydrophilic after oxidizing solution treatment (Supplementary Figs. 5a-c). With further investigations (Supplementary Figs. 5f-h), it can be confirmed that the hydrophilicity of oxidation treated Au/Fc-SAM/SLG surface is most probably due to the existent of complementary anions on the outside surface of graphene. Therefore, these investigations suggest that during the chemical oxidation treatment of Au/Fc-SAM/SLG, the Fc groups under graphene layer are oxidized to form Fc^+ cations, with balanced anions at the other side of graphene.

To benchmark the changes in charge transport through the Fc junction, with a large ON/OFF ratio due to chemical redox treatments, we constructed a tunnel junction in which the Fe-SAM was replaced by a C18-SAM and also characterised a graphene device without a SAM layer. When the latter benchmark devices are treated by same oxidizing solution, a slight increase of the conductance can be observed for both devices (Supplementary Figs. 7b and 8b), which is probably due to the increased conductance of the graphene layer. When the two devices are re-treated with a reducing solution, the conductances of the devices decrease. Such opposing responses and small conductance changes for the benchmark devices indicate that the responses of the Fc junction to oxidizing/reducing solutions come from the Fc-SAM layer. Furthermore, little response observed in the C18 junction indicates that the chemical redox treatments have negligible effect on the Au-S bonding and alkyl chains of SAM under the graphene layer, further confirming that the response of the Fc junction comes from the Fc groups.

When the Au/Fc-SAM/SLG is treated by H_2O_2 oxidation solution, hydroxyl groups (OH^-) are expected to form and adsorb on the surface of graphene. To explore the effect of OH^- adsorption, the Fc junction is treated by 0.1 M KOH solution for OH^- adsorption and 0.1 M HClO_4 solution for OH^- desorption. During the OH^- adsorption, a slight decrease of the J_D by a factor of less than two can be observed (Supplementary Fig. 9). Furthermore, the J_D of the Fc junction recovers to its initial value after the OH^- desorption treatment. Together these investigations confirm that the large ON/OFF ratio

switching of the Fc junction, in response to oxidizing/reducing solutions, is primarily attributed to the redox reactions of Fc groups in the Fc-SAM.

To confirm the path for the redox reaction between oxidant/reductant in the solution and Fc group in the junction, pristine thick layer (~3) graphene (Supplementary Fig. 4c) obtained by a peeling-off technique²³ was utilized to construct an Au/Fc-SAM/graphene junction. When the junction is treated by the same H₂O₂ oxidizing solution and NaBH₄ reducing solution, little response to the solutions can be observed (Supplementary Figs. 10a-c). This indicates that the chemical redox reactions of Fc groups in Au/Fc-SAM/graphene junction could only take place by crossing the single-layer graphene, but not the thick-layer graphene. Furthermore, possible reactions to the penetrated solution through the interface between graphene and SiO₂ substrate can also be ruled out. When the Fc junction is constructed with pristine SLG obtained from the peeling-off technique, the large ON/OFF-ratio switching of the junction by chemical redox treatments is realized (Supplementary Figs. 11a-c), which is similar to that of the Fc junction with a CVD-grown SLG. This confirms that the redox reaction between Fc groups and oxidant/reductant takes place through the perfect lattice of the graphene and not through defects in the graphene layer.

The redox reactions of the Fc-SAM in the Au/Fc-SAM/SLG junction were also investigated by electrochemical control. In this case, the applied electrochemical voltages can generate an electrochemical double layer at the outside surface of the graphene, which tunes the energy levels of the system, transfers electrons between Fc groups and Au electrode and thereby controls electrochemical redox reactions of Fc groups (Fig. 3a). First, the large area Au/Fc-SAM/SLG film is utilized as the working electrode for electrochemical characterization, with a Pt wire as counter electrode, a mercury/mercurous sulfate electrode (MSE) as the reference electrode and a 0.1 M HClO₄ solution as the electrolyte solution.

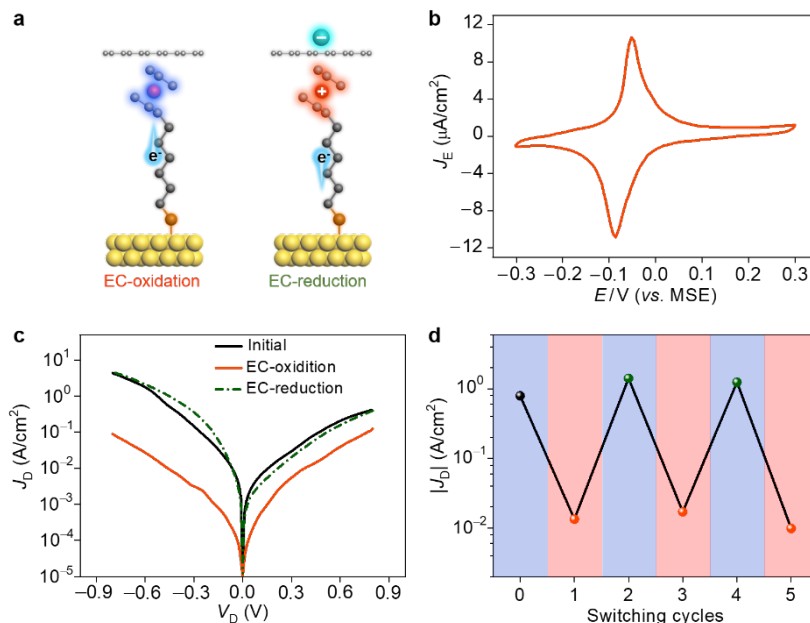


Fig. 3 | Electrochemical redox reactions of the junction. **a**, Schematic illustration of the electrochemical oxidation (EC-oxidation) and electrochemical reduction (EC-reduction) with controlled electron transfer processes. **b**, Cyclic voltammograms (CVs) for Au/Fc-SAM/SLG sample in 0.1 M HClO₄ solution. **c**, J_D – V_D curves for the junction in initial state, treated by EC-oxidation and re-treated by EC-reduction. **d**, Corresponding $|J_D|$ at $V_D = -0.5$ V for the junction sequentially treated by electrochemical oxidation (red) and reduction (green).

The cyclic voltammograms (CVs) of the Au/Fc-SAM/SLG sample (Fig. 3b) show a pair of redox peaks corresponding to the electrochemical redox reactions of Fc groups, with the peak position largely similar to that of the Au/Fc-SAM sample without a covering graphene layer (Supplementary Fig. 3). Furthermore, the CVs obtained for the Au/Fc-SAM/SLG sample show more simplified redox peaks with single peak properties, because the complex peak structures for Au/Fc-SAM sample (Supplementary Fig. 3) cannot be observed. This indicates that with a single layer of graphene between the Fc groups and electrolyte solution, more homogeneous electrochemical redox reactions take place. From contact angle characterizations, it can be observed that when the Au/Fc-SAM/SLG sample is electrochemically oxidized at 0.1 V (vs. MSE) for 180 s, the surface of Au/Fc-SAM/SLG becomes more hydrophilic (Supplementary Fig. 5d), which indicates that the electrochemically oxidized state has counter anions on the outside surface of graphene. When the oxidized sample is further

electrochemically reduced at -0.2 V (vs. MSE) for 180 s, the surface of Au/Fc-SAM/SLG recovers its hydrophilicity.

In the Au/Fc-SAM/SLG junctions, a graphene sheet is connected to ground and the drain voltage (V_D) is applied to Au film electrode. Two patterned platinum electrodes are laid around the functional center, where one is used as reference electrode and another one is used as counter electrode. The Au/Fc-SAM/SLG channel, reference and counter electrodes are covered by a small amount of 0.1 M HClO₄ solution for electrochemical redox reactions, then dried for measurements. When the junction is treated by electrochemical oxidation (EC-oxidation) at 0.3 V for 180 s, it can be observed that the original asymmetrical J_D - V_D curve with high conductance (Fig. 3c, black line) changes to a symmetrical J_D - V_D curve with low conductance (Fig. 3c, red line). This behaviour is similar to that observed under the chemical oxidation process (Fig. 2c). When the junction is re-treated by electrochemical reduction (EC-reduction) at -0.3 V for 180 s, the charge transport properties of the device almost recovers to its initial state (Fig. 3c, green dotted line). When the device is sequentially treated by electrochemical oxidation and reduction, as shown in Fig. 3d for $|J_D|$ at $V_D = -0.5$ V, the device reversibly switches between low conductance state in EC-oxidized state and high conductance state for EC-reduced state with high ON/OFF ratio of two orders of magnitude.

For the benchmark devices with a C18 SAM, or without a SAM, when the devices are treated by the same operation of electrochemical oxidation, only a slight increase of the current can be observed for both devices (Supplementary Figs. 7d and 8d). When the two devices are re-treated by the same operation of electrochemical reduction, the conductance of these devices slightly decrease after treatment (Supplementary Figs. 7e and 8e). These current changes are similar to those observed in response to chemical redox processes (Supplementary Figs. 7f and 8f). For the Fc-SAM/SLG junctions constructed by peeling off single-layer graphene and thick layer graphene, the responses of these devices to electrochemical redox treatments are also similar to those in response to chemical redox treatments (Supplementary Figs. 10 and 11). These

results indicate that the responses of the junction to electrochemical redox treatments come from the electrochemical redox reactions of Fc groups through graphene layer, similar to those in chemical redox processes.

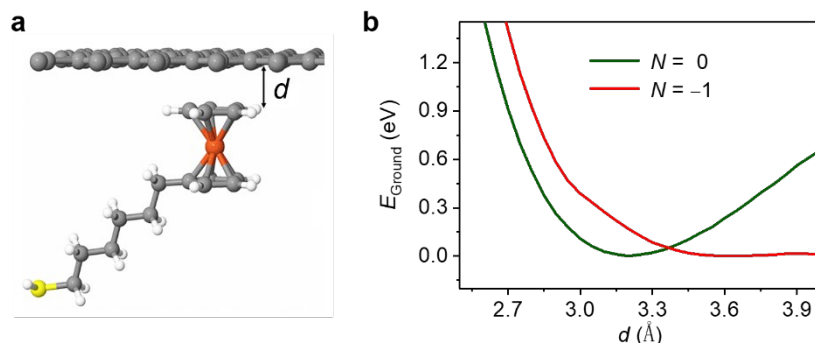


Fig. 4 | Graphene-molecule contact geometry. **a**, Schematic representation of the ferrocene-graphene contact, where d is the contact separation. **b**, Ground state energy versus d for different number of electrons N on the molecule, $N = 0$ (neutral) and $N = -1$ (oxidized).

To understand the redox tunable charge transport behavior in the Fc-SAM devices, we have developed a theoretical model by using a combination of density functional theory (DFT)²⁴ and quantum transport theory²⁵. This reveals that the lower conductance of the oxidized SAM is due to an increase in the separation between the top graphene contact and the Fc-SAM, resulting from their mutual electrostatic repulsion upon oxidation. Specifically, to construct a model of the device, the geometry of the isolated molecule was first optimised using the DFT code SIESTA. The geometry of each contact was optimised in the vicinity of an Au (111) surface and a graphene sheet separately. The thiol anchor group, attached to the alkane chain, binds to gold by losing a hydrogen and forms a covalent bond. The binding geometry of the ferrocene to the pristine undoped graphene was investigated. For the geometry of Fig. 4a, the plane of the 5 membered ring of the ferrocene unit lies parallel to the graphene surface. Using a VdW functional²⁶, the ground state energy was calculated as a function of separation d (Fig. 4b), and the minimum was found to occur at an optimum separation of $d = 3.2$ Å. Alternative geometries were considered (Supplementary Fig. 12), but found to be too low in conductance when compared with experiment (Supplementary Fig. 17). The behaviour of the graphene-ferrocene contact when the molecule becomes oxidized was

simulated by performing a net charge calculation on the graphene-ferrocene system as the number N of electrons in the junction of Fig. 4a was reduced. Upon oxidation, a Mulliken analysis shows the number of electrons on the ferrocene to be $N = -1$ (supplementary note 3). Figure 4b shows that as the ferrocene becomes oxidized, the minimum of the energy curve shifts from $d = 3.2 \text{ \AA}$ for the neutral molecule to a value of 3.8 \AA , in agreement with previous work that showed that oxidation of a ferrocene unit leads to an electrostatic repulsion between the positively charged ferrocene and the positively charged graphene layer⁶. We also calculated the binding energy when the graphene surface is doped with hydroxide molecules, which remove electrons from the graphene so that they become OH^- ions. In this case, the graphene becomes positively charged, which is accordance with experimental results of XPS characterization (Supplementary Fig. 2c). This also changes the charge state on the ferrocene (Supplementary Fig. 14) and prevents binding for all calculated values of d , consistent with electrostatic repulsion at the contact.

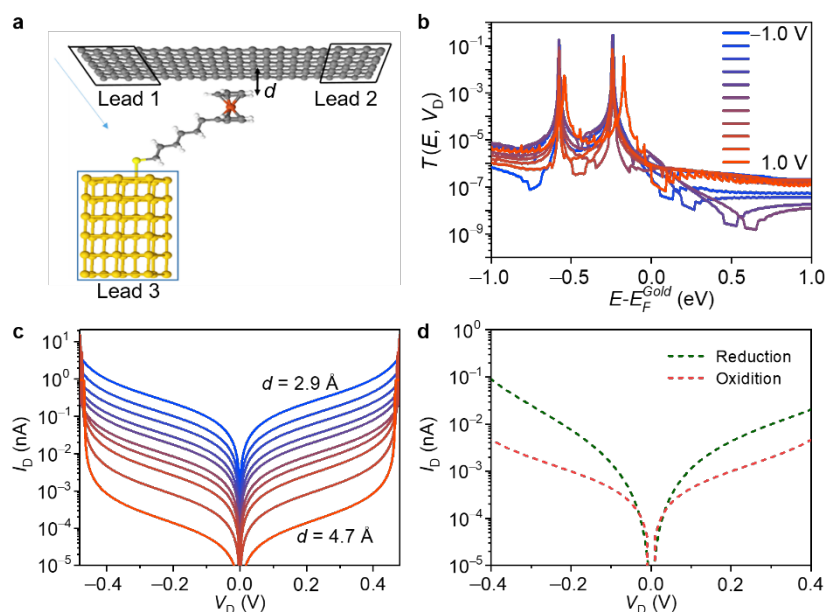


Fig. 5 | Theoretical model of junction. **a**, Schematic representation of the three-terminal gold-molecule-graphene junction with periodic boundary conditions along the y -axis. **b**, Transmission coefficient $T(E, V_D)$ for source drain voltages between -1 and 1 V with step of 0.2 V for $d = 3.2 \text{ \AA}$. **c**, I - V characteristics for contact distances of d changed from 2.9 to 4.7 Å with step of 0.2 Å. **d**, Comparison between the current for reduction state (green curve, $d = 3.2 \text{ \AA}$) and the current for oxidation state (red curve,

$d = 3.8 \text{ \AA}$).

To calculate the electrical current through the SAM, we model the junction shown in Fig. 5a. The in-plane periodicity of the graphene and the molecular layer is achieved by repeating the unit cell using a Bravais lattice with 30k-points in the y -direction. This models a SAM, in which the molecules are $\sim 2 \text{ nm}$ apart. The gold electrode is modelled as a nanowire attached to each molecule. A mean-field Hamiltonian and an overlap matrix were extracted from the converged DFT calculation and combined with our quantum transport calculation code, Gollum, to calculate the voltage-dependent transmission coefficient $T(E, V_D)$ of electrons of energy E passing from the graphene to gold electrodes in the presence of a source-drain voltage V_D . More details of the theoretical method are provided in the Supplementary Section 3.

The resulting voltage-dependent transmission curves $T(E, V_D)$ for a contact separation $d = 3.2 \text{ \AA}$ are shown in Fig. 5b. In these plots, the HOMO resonance (at $E - E_F^{Gold} = -0.25 \text{ eV}$) of the molecule lies close to the Fermi energy E_F^{Gold} of the gold electrode, and the voltage-dependent minimum in the transmission corresponds to the Dirac point of the graphene. The voltage dependence is calculated by applying a potential gradient to the Hamiltonian elements of the graphene leads, which for negative V_D causes the Dirac point to shift to higher energies and the HOMO to slightly lower energies. The source drain current is then evaluated by the Landauer formula:

$$I(V_D) = \frac{2e}{h} \int_{E_F^{Gold}}^{E_F^{Gr}(V_D)} T(E, V_D) dE$$

Since the gold lead is earthed, the gold Fermi energy E_F^{Gold} is not affected by the source-drain or gate voltage. If the graphene-ferrocene distance d is held fixed, the resulting I-V curve is shown in Fig. 5d (green curve) and reveals that there is a small rectification with a larger negative bias current than positive current. This follows the behaviour of the initial – pre-oxidized experimental measurement (Figs. 2c and 3c).

To model the behaviour of the SAM upon oxidation, we account for electrostatic repulsion between the oxidized ferrocene and graphene by increasing the contact separation d . Doping of the graphene also causes the Dirac point to be shifted away

from its position for neutral graphene, which removes the dip in the transmission curves close to the Fermi energy and causes the I - V curves to become symmetric. The resulting current-voltage curves for different separations d (Fig. 5c) show a decrease in current of 2 orders of magnitude occurs when the distance d increases from 3.2 to 3.8 Å. Figure 5d then shows a comparison between the contact separation 3.2 Å (reduced) and 3.8 Å (oxidized), which shows good agreement to the experimental results of Fig. 2c. Therefore, the reduction in current through the device when the molecule is oxidized is due to an increase in the separation between the top graphene contact and the Fc-SAM, resulting from their mutual electrostatic repulsion in the oxidized state.

In summary, we have demonstrated redox control of cross-plane charge transport in an Au/Fc-SAM/SLG junction. Specifically, an oxidant/reductant or an electrochemical potential induces redox reactions of Fc groups under the graphene and changes the separation between the top graphene contact and the Fc-SAM. This switches the junction between a high conductance neutral state with an asymmetrical J_D - V_D curve and a low conductance oxidized state with a symmetrical J_D - V_D curve, yielding a large ON/OFF ratio exceeding two orders of magnitude. During these redox reactions, charges cross the graphene layer. Due to the electronic transparency and ion impermeability of graphene in most cases, in the oxidized state, the counter anions remain separated on the top surface of the graphene layer and balance the oxidized Fc cations beneath graphene. Therefore, the vertical Au/SAM/graphene junction can be used to explore chemical and electrochemical reactions at graphene heterointerface, which are sensitive to unique selective permeability properties of the graphene membrane^{18,20,27}. Furthermore, by utilizing the selective permeability of graphene to charges and ions, the states of the SAMs can be effectively tuned by external stimuli, which moves us a significant step closer to realizing new functionalities for molecular electronics devices, such as chemical/biological sensors, electrochemical detectors, optoelectronic devices and logical devices.

References

1. Vilan, A., Aswal, D. & Cahen, D. Large-area, ensemble molecular electronics: motivation and challenges. *Chem. Rev.* **117**, 4248–4286 (2017).
2. Xiang, D., Wang, X., Jia, C., Lee, T. & Guo, X. Molecular-scale electronics: from concept to function. *Chem. Rev.* **116**, 4318–4440 (2016).
3. Xin, N. *et al.* Concepts in the design and engineering of single-molecule electronic devices. *Nat. Rev. Phys.* **1**, 211–230 (2019).
4. Jia, C. C., Ma, B. J., Xin, N. & Guo, X. F. Carbon electrode-molecule junctions: a reliable platform for molecular electronics. *Acc. Chem. Res.* **48**, 2565–2575 (2015).
5. Capozzi, B. *et al.* Single-molecule diodes with high rectification ratios through environmental control. *Nat. Nanotechnol.* **10**, 522–527 (2015).
6. Chen, X. P. *et al.* Molecular diodes with rectification ratios exceeding 10^5 driven by electrostatic interactions. *Nat. Nanotechnol.* **12**, 797–803 (2017).
7. Jia, C. *et al.* Covalently bonded single-molecule junctions with stable and reversible photoswitched conductivity. *Science* **352**, 1443–1445 (2016).
8. Xin, N. *et al.* Thermally activated tunneling transition in a photoswitchable single-molecule electrical junction. *J. Phys. Chem. Lett.* **8**, 2849–2854 (2017).
9. Perrin, M. L., Burzuri, E. & van der Zant, H. S. J. Single-molecule transistors. *Chem. Soc. Rev.* **44**, 902–919 (2015).
10. Xin, N. *et al.* Tuning charge transport in aromatic-ring single-molecule junctions via ionic-liquid gating. *Angew. Chem. Int. Ed.* **57**, 14026–14031 (2018).
11. Lambert, C. J. Basic concepts of quantum interference and electron transport in single-molecule electronics. *Chem. Soc. Rev.* **44**, 875–888 (2015).
12. Liu, J. Y., Huang, X. Y., Wang, F. & Hong, W. J. Quantum interference effects in charge transport through single-molecule junctions: detection, manipulation, and application. *Acc. Chem. Res.* **52**, 151–160 (2019).
13. Jia, C. *et al.* Quantum interference mediated vertical molecular tunneling transistors. *Sci. Adv.* **4**, eaat8237 (2018).
14. Famili, M. *et al.* Self-assembled molecular-electronic films controlled by room temperature quantum interference. *Chem* **5**, 474–484 (2019).
15. Rincon-Garcia, L., Evangelini, C., Rubio-Bollinger, G. & Agrait, N. Thermopower

- measurements in molecular junctions. *Chem. Soc. Rev.* **45**, 4285–4306 (2016).
16. Gu, C. H., Jia, C. C. & Guo, X. F. Single-molecule electrical detection with real-time label-free capability and ultrasensitivity. *Small Methods* **1**, 1700071 (2017).
 17. Guan, J. *et al.* Direct single-molecule dynamic detection of chemical reactions. *Sci. Adv.* **4**, eaar2177 (2018).
 18. Jia, C. C. *et al.* High-efficiency selective electron tunnelling in a heterostructure photovoltaic diode. *Nano Lett.* **16**, 3600–3606 (2016).
 19. Jia, C. C. *et al.* High-efficiency photovoltaic conversion at selective electron tunneling heterointerfaces. *Adv. Electron. Mater.* **3**, 1700211 (2017).
 20. Lozada-Hidalgo, M. *et al.* Sieving hydrogen isotopes through two-dimensional crystals. *Science* **351**, 68–70 (2016).
 21. Abbott, N. L. & Whitesides, G. M. Potential-dependent wetting of aqueous-solutions on self-assembled monolayers formed from 15-(ferrocenylcarbonyl)pentadecanethiol on gold. *Langmuir* **10**, 1493–1497 (1994).
 22. Jia, C., Jiang, J., Gan, L. & Guo, X. Direct optical characterization of graphene growth and domains on growth substrates. *Sci. Rep.* **2**, 707 (2012).
 23. Ma, B., Ren, S., Wang, P., Jia, C. & Guo, X. Precise control of graphene etching by remote hydrogen plasma. *Nano Res.* **12**, 137–142 (2019).
 24. Soler, J. M. *et al.* The SIESTA method for ab initio order-N materials simulation. *J. Phys.: Condens. Matter* **14**, 2745–2779 (2002).
 25. Ferrer, J. *et al.* GOLLUM: a next-generation simulation tool for electron, thermal and spin transport. *New J. Phys.* **16**, 093029 (2014).
 26. Dion, M. *et al.* Van der Waals density functional for general geometries. *Phys. Rev. Lett.* **92**, 246401 (2004).
 27. Fu, Y., Rudnev, A. V., Wiberg, G. K. & Arenz, M. Single graphene layer on Pt (111) creates confined electrochemical environment via selective ion transport. *Angew. Chem. Int. Ed.* **56**, 12883–12887 (2017).

Acknowledgements

X.D. acknowledges financial support by National Science Foundation DMR1508144. Y.H. acknowledges financial support by National Science Foundation EFRI-1433541. Support from the UK EPSRC is acknowledged, through grant nos. EP/N017188/1, EP/M014452/1, EP/P027156/1 and EP/N03337X/1. Support from the European Commission is provided by the FET Open project 767187 – QuIET.

Author contributions

X.D., C.L. and C.J. conceived and designed the experiments. C.J. performed most of the experiments including device fabrication, characterization and data analysis. I.G. and A.A. performed the theoretical simulation and data analysis. P.W., Z.H., Y.W., P.C., L.W., J.Z., Z.F. and Z.Z. assisted with device fabrication and characterization. X.D., C.L. and Y.H. supervised the research. X.D., C.L., C.J. and I.G. co-wrote the paper. All authors discussed the results and commented on the manuscript.

Additional information

Supplementary information is available in the online version of the paper. Reprints and permissions information is available online at www.nature.com/reprints. Publisher's note: Springer Nature remains neutral with regard to jurisdictional claims in published maps and institutional affiliations. Correspondence and requests for materials should be addressed to X.D. and C.L.

Competing financial interests

The authors declare no competing financial interests.

Methods

Device fabrication. The device fabrication processes were similar to our previous works^{13,14}. Specifically, silicon wafer (single side polished, highly *n*-doped, coated with 300 nm SiO₂) was cut into appropriate size and cleaned for further use. A photoresist mask with patterned 80 μm holes was covered on the silicon wafer by a photolithography process (Karl Suss MA6 Contact Aligner). The 300 nm SiO₂ layer in the holes was then selectively etched with a buffered oxide etchant (BOE, 1:6 HF:NH₄F) for 6 minutes. Next, a 30 nm SiO₂ layer was thermally grown on the exposed silicon surface in the holes by annealing in air at 960 °C for 45 minutes. With another photolithography process and e-beam evaporation, 10/60 nm Ti/Pt gate electrodes and metal marks were placed around the pretreated holes. After e-beam lithography, BOE etching and e-beam evaporation processes, the conductive silicon surface in three 1.5×1.5 μm² square holes at the center of 80 μm holes were exposed out again and further covered with ultra-flat 5/23 nm Ti/Au film. After that, the prepared samples were annealed at 300 °C for 1 h and stored in a vacuum desiccator for further use.

For molecule self-assembling on the surface of the gold films, 1 mM solution of the 6-ferrocenylhexanethiol (FcC₆S) in the chromatographic grade ethanol was prepared in the glove box (< 1 ppm O₂/H₂O). The pretreated sample was immersed in 5 ml corresponding FcC₆S solution for 24 h. After that, the sample was taken out, alternately washed with hexane and ethanol for three times and dried by a nitrogen blow. For the contrast system, 1-octadecanethiol (C18) was self-assembling on the surface of the gold film by same processes.

High-quality single layer graphene (SLG) was synthesized by a low-pressure chemical vapor deposition (CVD) method²² and transferred on the samples by a poly(methyl methacrylate) (PMMA) assisted wet transfer process. Next, patterned graphene sheets were formed with covering the 80 μm holes by a photolithography process and selective oxygen plasma etching. After a photolithography process, 20/60 nm Ti/Au was thermally evaporated for fabrication of the drain electrodes with connecting to the graphene panels and the source electrodes at the corner, which is connected to the back conductive silicon layer. For the contrast devices with pristine

graphene, the devices were fabricated by similar processes, where the pristine graphene was obtained by a peeling-off technique^{23,28} and transferred on the samples by a precise transfer technique²⁹. All prepared devices were stored in a vacuum desiccator for further measurements.

Device characterization. Electrical properties of the devices were measured by an Agilent 5155C semiconductor characterization system on a Model TTPX cryogenic probe station (Lake Shore Cryotronics, Inc.). Electrochemical characterizations were implemented on a CHI660E electrochemical station. X-ray photoelectron spectroscopy (XPS) characterizations were carried out on Kratos Axis Ultra X-ray photoelectron spectroscopy system (AlK α radiation, power \leq 180 W). LabRAM HR Evolution Raman spectrometer (Horiba Scientific) with excitation wavelength at 488 nm was used for Raman characterizations. Contact angle characteristics were measured by using a telescope and goniometer (Ramé-Hart) from water drops that were dropped to the surface using a micrometric syringe.

Theoretical calculations. The theoretical calculations were carried out by using a combination of density functional theory (DFT)²⁴ and quantum transport theory²⁵. Specifically, the geometry of the ferrocene molecule was calculated by relaxing the geometry in SIESTA, until all forces on the atoms were less than 0.01 V/Å. Here, a double zeta basis set was used, along with norm-conserving pseudopotentials, the local density approximation²⁵ was used to describe the exchange correlational functional and the energy cutoff was 150 Ry. The same parameters were also used to optimize the geometry of the graphene sheet which consisted of 72 atoms and utilized periodic boundary conditions. To calculate the binding energy using SIESTA we use a counterpoise method to correct for basis set superposition errors that are inherent with the localized orbital basis sets employed here. The calculations of the transport properties were performed using the local-density approximation (LDA) functional of the exchange and correlation functional is used with the CA parameterization along with a double- ζ polarized (DZP) basis set, a real-space grid defined with an equivalent energy cut-off of 150 Ry. Detailed explanations of the theoretical calculations are given out in Supplementary Section 3.

References

28. Jia, C. *et al.* Logic control of interface-induced charge-trapping effect for ultrasensitive gas detection with all-mirror-image symmetry. *Adv. Mater. Technol.* **1**, 1600067 (2016).
29. Yu, W. J. *et al.* Vertically stacked multi-heterostructures of layered materials for logic transistors and complementary inverters. *Nat. Mater.* **12**, 246–252 (2013).